Office of Naval Research
Contract N00014-88-K-0472
R T Code 413p008

Technical Report No. 4

HOST-GUEST PREORGANIZATION AND COMPLEMENTARITY: A MOLECULAR MECHANICS AND MOLECULAR DYNAMICS STUDY OF CATION COMPLEXES OF A CYCLIC UREA-ANISOLE SPHERAND.

by

Peter V. Maye and Carol A. Venanzi

Prepared for Publication in

Journal Of The American Chemical Society

New Jersey Institute of Technology
Chemistry Division
Newark, NJ 07102

April 30, 1990

SECURITY CLASSIFICATION OF THIS PAGE

REPORT DOCUMENTATION PAGE

Form Approved OMB No 0704-0188

1a REPORT SECURITY CLASSIFICATION: Unclassified	1b RESTRICTIVE MARKINGS
2a SECURITY CLASSIFICATION AUTHORITY	3 DISTRIBUTION / AVAILABILITY OF REPORT
2b DECLASSIFICATION / DOWNGRADING SCHEDULE	
4 PERFORMING ORGANIZATION REPORT NUMBER(S)	5 MONITORING ORGANIZATION REPORT NUMBER(S)
6a NAME OF PERFORMING ORGANIZATION: New Jersey Institute of Technology; 6b OFFICE SYMBOL (If applicable)	7a NAME OF MONITORING ORGANIZATION
6c ADDRESS (City, State, and ZIP Code): Chemistry Division, University Heights, Newark, New Jersey 07102	7b ADDRESS (City, State, and ZIP Code)
8a NAME OF FUNDING / SPONSORING ORGANIZATION: Office of Naval Research; 8b OFFICE SYMBOL (If applicable): ONR	9 PROCUREMENT INSTRUMENT IDENTIFICATION NUMBER
8c ADDRESS (City, State, and ZIP Code): 800 N. Quincy Street, Arlington, UA 22217-5000	10 SOURCE OF FUNDING NUMBERS: PROGRAM ELEMENT NO. / PROJECT NO. / TASK NO. / WORK UNIT ACCESSION NO.

11 TITLE (Include Security Classification)
Host-Guest Preorganization and Complementarity: A Molecular Mechanics and Molecular Dynamics Study of Cation Complexes of a Cyclic Urea-Anisole Spherand.

12 PERSONAL AUTHOR(S)
Peter V. Maye and Carol A. Venanzi

13a TYPE OF REPORT	13b TIME COVERED	14 DATE OF REPORT (Year, Month, Day)	15 PAGE COUNT
Manuscript	FROM _____ TO _____	April 30, 1990	67

16 SUPPLEMENTARY NOTATION
Prepared for Publication in Journal of the American Chemical Society

17 COSATI CODES			18 SUBJECT TERMS (Continue on reverse if necessary and identify by block number)
FIELD	GROUP	SUB-GROUP	
07	03		

19 ABSTRACT (Continue on reverse if necessary and identify by block number)

Cram and coworkers have optimized the binding efficiency of spherands for their cationic guests by using the principles of preorganization and complementarity to guide the design of the molecular architecture of these macrocyclic hosts. In the present work, we provide a quantitative interpretation of these principles in terms of the inter- and intramolecular energy components associated with the formation of the host-guest complex. To that end, molecular mechanics energy optimizations and molecular dynamics simulations are carried out for 1 and for the complexes of 1 with alkali metal cations and t-BuNH$_3^+$. Host preorganization is interpreted in terms of the spherand reorganization energy, that is, the change in the strain and nonbonded energy of the spherand upon complexation. Electrostatic complementarity is explored by evaluation of the change upon complexation in: (1) the electrostatic component of the ion-spherand interaction energy and (2) the molecular electrostatic potential pattern presented by the spherand to the guest.

ORGANIC CHEMISTRY

20 DISTRIBUTION / AVAILABILITY OF ABSTRACT	21 ABSTRACT SECURITY CLASSIFICATION
☑ UNCLASSIFIED/UNLIMITED ☐ SAME AS RPT. ☐ DTIC USERS	Unclassified

22a NAME OF RESPONSIBLE INDIVIDUAL	22b TELEPHONE (Include Area Code)	22c OFFICE SYMBOL
Harold E. Guard	(202) 696-4402	ONR

DD Form 1473, JUN 86 — Previous editions are obsolete. — SECURITY CLASSIFICATION OF THIS PAGE

The calculations show that the net favorable complexation energy is the result of the offset of the unfavorable reorganization energy of the spherand by the overwhelmingly favorable electrostatic component of the ion-spherand interaction energy. The results indicate that the spherand must undergo a larger conformational change to complex the smaller cations. But for all the cations complexed, the unfavorable reorganization energy is offset by a large increase in the electrostatic complementarity of the ion binding site when the spherand adopts its complexed conformation.

HOST-GUEST PREORGANIZATION AND COMPLEMENTARITY: A MOLECULAR MECHANICS AND MOLECULAR DYNAMICS STUDY OF CATION COMPLEXES OF A CYCLIC UREA-ANISOLE SPHERAND

P.V. Maye[+] and C.A. Venanzi[*]

Department of Chemical Engineering, Chemistry,

and Environmental Science

New Jersey Institute of Technology

University Heights

Newark, NJ 07102

[+]Present address: The BOC Group, Pharmaceuticals R & D Division,

100 Mountain Ave., Murray Hill, NJ 07974

[*]Author to whom correspondence should be addressed.

ABSTRACT

Cram and coworkers have optimized the binding efficiency of spherands for their cationic guests by using the principles of preorganization and complementarity to guide the design of the molecular architecture of these macrocyclic hosts. In the present work, we provide a quantitative interpretation of these principles in terms of the inter- and intramolecular energy components associated with the formation of the host-guest complex. To that end, molecular mechanics energy optimizations and molecular dynamics simulations are carried out for **1** and for the complexes of **1** with alkali metal cations and $\underline{t}$-$BuNH_3^+$. Host preorganization is interpreted in terms of the spherand reorganization energy, that is, the change in the strain and nonbonded energy of the spherand upon complexation. Electrostatic complementarity is explored by evaluation of the change upon complexation in: (1) the electrostatic component of the ion-spherand interaction energy and (2) the molecular electrostatic potential pattern presented by the spherand to the guest. The calculations show that the net favorable complexation energy is the result of the offset of the unfavorable reorganization energy of the spherand by the overwhelmingly favorable electrostatic component of the ion-spherand interaction energy. The results indicate that the spherand must undergo a larger conformational change to complex the smaller cations. But for all the cations complexed, the unfavorable reorganization energy is offset by a large increase in the electrostatic complementarity of the ion binding site when the spherand adopts its complexed conformation.

INTRODUCTION

Cram and coworkers have synthesized a class of macrocyclic spherands which are highly efficient complexing hosts for certain cations.[1-4] These molecules are composed of anisole fragments linked into six-membered macrocycles; the anisoles may be replaced by phenyl fragments or cyclic urea fragments, and may be bridged by ether groups. Spherands have rigid structures which form cavities containing electron-rich oxygen atoms suitable for binding guests such as alkali metal and alkylammonium cations.

The spherand **1** is composed of three cyclic urea

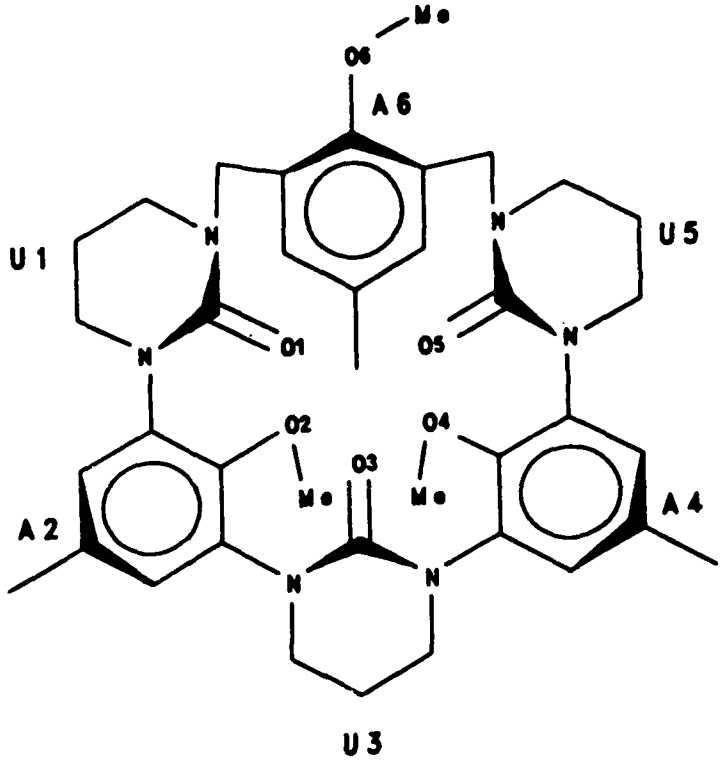

fragments (U1, U3 and U5) alternating with three anisole fragments (A2, A4 and A6) in the macrocycle. Fragment A6 is substituted with methylene groups at the 2- and 6- positions. Spherand 1 has been shown by Cram et al[5,6] to be an especially effective complexing agent for alkali metal and other cations. For example, for extraction of alkali metal and alkylammonium picrate salts from D_2O into $CDCl_3$ at 25^0C, the binding free energies of 1 with the guests Li^+, Na^+, K^+, Rb^+, Cs^+, and $\underline{t}$-$BuNH_3^+$ are 12.1, 15.4, 15.6, 14.2, 13.1, and 13.2 Kcal/mol, respectively[5,6]. In addition, a series of mimics of the proteolytic enzyme alpha-chymotrypsin has been built from 1 by incrementally attaching molecular fragments which chemically mimic the active site of the native enzyme; the spherand itself serves as the binding site[7-9].

The basis for the high cation affinity of 1 was previously studied in this laboratory using molecular modeling techniques[10-12]. It was shown that the spherand had a high degree of electrostatic complementarity for its $\underline{t}$-$BuNH_3^+$ guest. The electrostatic potential surface of the spherand was found to be well matched to the electrostatic potential surface of the ammonium hydrogens, which perch tripod fashion on the carbonyl oxygens in the complex. Additional work in this laboratory[13,14] has concentrated on the structure-function relationships of alpha-chymotrypsin mimics constructed using this spherand as a template for the binding site. Kollman and coworkers have studied the complexation of cationic guests by anisole spherands[15] and by more flexible 18-crown-6 ethers[16].

Cram and coworkers have optimized the binding affinity of the spherands for their cationic guests by using the principles of preorganization and complementarity[17] to guide the design of the molecular architecture of the macrocyclic hosts. The principal of preorganization states that "the more highly hosts and guests are organized for binding and for low solvation prior to their complexation, the more stable will be their complexes"[3]. In other words, the spherand should be organized during synthesis rather than during complexation into a conformation which will optimally bind the guest. In addition, the solvent molecules should undergo very little positional reorganization during complexation. The principle of complementarity states that "in complexes of substantial stability, the binding sites of host and guest components must simultaneously contact and attract one another"[3]. By applying these principles to the inspection of CPK molecular models, the Cram group has conceived and implemented the design of several successful spherands.

It is the purpose of the present work to provide a quantitative interpretation of the principles of complementarity and preorganization in terms of the inter- and intramolecular energy components associated with the formation of the host-guest complex. To that end, molecular mechanics energy optimizations and molecular dynamics simulations are carried out for 1 and for the complexes of 1 with Li^+, Na^+, K^+, Rb^+, Cs^+ and $\underline{t}$-$BuNH_3^+$ cations. In the present paper, the principle of preorganization is interpreted in terms of the change in the reorganization energy of the spherand upon complexation. This quantity is obtained as the

difference in the spherand intramolecular strain and nonbonded energy before and after complexation. It is visualized through the changes in the inter-ring dihedral angles of the spherand. In a future publication, preorganization will be further analyzed in terms of the solvent reorganization that accompanies host-guest complexation.

The principle of complementarity is interpreted in several ways. Calculation of the distance between the complexed cation and the spherand oxygens gives a measure of the ability of the spherand atoms to form optimal van der Waals contact with the guest. Calculation of the intermolecular electrostatic, van der Waals, and hydrogen bonding energy of the host-guest complex allows evaluation of the nonbonded contributions to the energy of the complex. In particular, the significance of the electrostatic component in promoting the ability of the host to attract the guest is explored by evaluation of the change in the electrostatic component of the ion-spherand interaction energy and by comparison of the molecular electrostatic potential pattern presented by the host to the guest when the spherand adopts its complexed versus its uncomplexed conformation.

The net effect of the interrelated principles of complementarity and preorganization is assessed through the evaluation of the complexation energy. This quantity reflects the energetic trade-off between the unfavorable reorganization energy of the spherand upon complexation and the favorable nonbonded intermolecular interaction energy of the host-guest complex.

METHODOLOGY

Force Field Parameters. The energy optimizations and molecular dynamics simulations were carried out with the AMBER 3.0 molecular modeling package[18]. The AMBER united atom force field[19] was supplemented with parameters for the spherand, as described in reference 12. "Potential-derived"[20] partial atomic charges were obtained by separately fitting atom-centered point charges to reproduce the STO-3G electrostatic potential surface of the individual anisole and cyclic urea fragments of the spherand. The Gaussian80 UCSF package[21] was used to carry out the calculations. The fragments were defined so as to take into account the effect of the presence of neighboring fragments on the charge distribution of a particular cyclic urea or anisole ring. These extended fragments were N-ethyl-N'-methyl cyclic urea (for U1 and U5), N,N'-dimethyl cyclic urea (for U3), 2,6-di(N-methylformamido)-4-methylanisole (for A2 and A4) and 2,4,6-trimethylanisole (for A6). The charges obtained for each fragment were then scaled by a factor of 1.13 in order to approximate a set of 6-31G** potential derived charges[22].

The fragments were then assembled into the complete spherand. For those atoms located in regions where two extended fragments overlapped, the partial atomic charges were averaged. The atomic charges were then summed, resulting in a residual positive charge on the spherand. This residual charge was removed by the following procedure: (1) The largest positive atomic charge was identified; (2) For each atom, the charge difference between the largest charge and the individual atomic charge was calculated; (3) The charge on each atom was adjusted by subtracting from it the charge difference

in step (2) multiplied by the spherand's residual positive charge divided by the sum of all the charge differences.

The force field of References 11 and 12 was also used for t-$BuNH_3^+$. The partial atomic charges for this cation were determined by fitting atomic point charges to reproduce the STO-3G electrostatic potential surface of the molecule. The charges were left unscaled since the molecule is a cation. The Van der Waals parameters used for the alkali metal cations were those of Grootenhuis and Kollman[23]; these ions were assigned a charge of plus one.

Complexation Energetics. The AMBER force field used in the molecular mechanics and molecular dynamics calculations described below is defined in Eqn. (1).

$$E_T = \sum_{bonds} K_R(R - R_o)^2 + \sum_{angles} K_\theta(\theta - \theta_o)^2 + \sum_{dihedrals} V_n/2[1 + \cos(n\phi - \gamma)] + \sum_{i<j}[A_{ij}/R_{ij}^{12} - B_{ij}/R_{ij}^{6} + q_iq_j/\varepsilon R_{ij}] + \sum_{H-bonds}[C_{ij}/R_{ij}^{12} - D_{ij}/R_{ij}^{10}] \quad (1a)$$

$$= E_{STR} + E_{VDW} + E_{EL} + E_{HB} \quad (1b)$$

This equation gives the total molecular mechanics energy of a molecule, or a molecular complex, as the sum of strain (bond stretching, angle bending, and torsional) contributions (E_{STR}), as well as Van der Waals (E_{VDW}), electrostatic (E_{EEL}), and hydrogen bonding (E_{HB}) energy components. The total intramolecular energy of the spherand, for example, is given by Eqn. (1), where i and j refer to the spherand atoms only. E_S, refers to the energy calculated by Eqn. (1) for the uncomplexed spherand; E_S refers to the energy of the spherand in the ion-spherand complex. Similarly, E_I and E_I, refer to the total intramolecular energy of the t-$BuNH_3^+$ cation calculated by Eqn. (1) for the complexed and uncomplexed ligand, respectively. (These terms equal zero for the alkali metal cations.) The total energy of the ion-spherand complex, E_T, is given by Eqn. (2),

$$E_T = E_S + E_I + E_{IS} \qquad (2)$$

where E_{IS} is the non-bonded component of the ion-spherand interaction energy. E_{IS} is defined in Eqn. (3)

$$E_{IS} = E_{VDW}(IS) + E_{EL}(IS) + E_{HB}(IS) \qquad (3)$$

as the sum of only the intermolecular van der Waals (E_{VDW}), electrostatic (E_{EL}), and hydrogen bonding (E_{HB}) terms of Eqn. (1), where i and j refer, in this context, to the spherand and cation atoms, respectively.

From these relationships, the spherand reorganization energy, $E_{RE}(S)$, can be defined by Eqn. (4a)

$$E_{RE}(S) = E_S - E_{S'} \qquad (4a)$$

as the difference between the energy of the spherand in the ion-spherand complex, E_S, and the energy of the uncomplexed spherand, $E_{S'}$. This is equivalent to the sum of changes upon complexation in the spherand's intramolecular strain (ΔE_{STR}), van der Waals (ΔE_{VDW}), electrostatic (ΔE_{EL}), and hydrogen bonding (ΔE_{HB}) energy components as shown in Eqn. (4b).

$$E_{RE}(S) = \Delta E_{STR}(S) + \Delta E_{VDW}(S) + \Delta E_{EL}(S) + \Delta E_{HB}(S) \qquad (4b)$$

The reorganization energy of the t-$BuNH_3^+$ cation, $E_{RE}(I)$, is calculated from an expression equivalent to Eqn. (4). For the alkali metal cations, of course, this quantity is zero.

Finally, Eqn. (5a) defines E_C, the energy of complexation, as the difference between the total energy, E_T, of the ion-spherand complex and the energies of the uncomplexed ion and spherand.

$$E_C = E_T - E_{S'} - E_{I'} \qquad (5a)$$

Eqn. (5b)

$$= E_{IS} + E_{RE}(S) + E_{RE}(I) \qquad (5b)$$

gives the equivalent expression for E_C in terms of the spherand and ion reorganization energies, $E_{RE}(S)$ and $E_{RE}(I)$, and the intermolecular energy component of E_T, E_{IS}.

Molecular Mechanics Energy Minimization. The starting structures for energy minimization of 1 and of the cation complexes of 1 were obtained from the X-ray structure of the spherand complexed with $\underline{t}$-$BuNH_3^+$ provided by K.N. Trueblood[24]. To obtain the starting structure of the uncomplexed spherand, the atomic coordinates of the ligand were deleted from the X-ray structure. Then, the spherand coordinates were subjected to full conjugate gradient energy minimization. This structure was subsequently used to construct the starting structure for the optimization of the alkali metal ion complexes in which each of the five metal ions was "perched" atop the carbonyl oxygens of the spherand in a position 4.0 Å equidistant from each oxygen. For the optimization of the complex of 1 with $\underline{t}$-$BuNH_3^+$, the X-ray structure[24] was used as the starting structure. Then, each of the six complexes was subjected to a full conjugate gradient energy minimization. All optimizations were terminated when the root mean square of the conformational energy gradient reached 0.0005 Kcal/mol-Å.

Molecular Dynamics Simulations. The initial geometries for the molecular dynamics simulations were the energy-optimized structures determined above. Three trajectories apiece were calculated for the uncomplexed spherand and for each of the six ion-spherand complexes. Each trajectory consisted of 50 picoseconds (ps) of equilibration followed by 100 ps of data collection, resulting in 300 ps of simulation data for analysis of each

molecular system. The three different trajectories for each system were generated by using different sets of initial atomic velocities. The simulations were carried out at a constant temperature of 300° via coupling to a heat bath[25] and the bond lengths were constrained to their molecular mechanics optimized values using the SHAKE algorithm[26]. Stepsizes of 0.5 femtosecond (fs) were used and the molecular geometry was saved every 50 fs.

From the 300 ps of simulation data accumulated for each molecular system, average energetic and structural quantities such as ion-spherand oxygen distances, oxygen-oxygen distances, and inter-ring dihedral angles were calculated. The inter-ring dihedral angles were defined by the angle formed by the carbonyl carbon (of U1, U3, or U5), nitrogen (of U1, U3, or U5), carbon (at position 2 of A2, A4, or A6), and carbon (at position 1 of A2, A4, or A6). Therefore, the methylene bridges were ignored in the definition of the A6-U1 and A6-U5 inter-ring dihedral angles.

During analysis of the complexes, it appeared that the complex of **1** with Li^+ was exploring a region of the conformational potential energy surface that was considerably different from the molecular mechanics structure of the complex. For direct comparison with the molecular mechanics results, the coordinates of the time-averaged molecular dynamics Li^+-**1** complex were optimized and the results are presented in the molecular mechanics tables below.

Molecular Electrostatic Potential Patterns. Molecular electrostatic potential (MEP) patterns were calculated for the spherand geometry taken from each of the six cation-spherand

complexes in the molecular mechanics study described above. The coordinates of the ligands and their associated charges were deleted. The molecular electrostatic potential energy was determined by calculating the Coulombic interaction between the spherand and a unit positive point charge positioned at grid points throughout the plane. Therefore, the maps represent an evaluation of $E_{EL}(IS)$ for the spherand-point charge (or alkali metal cation) interaction at various points in the plane. The maps are a representation of the molecular electrostatic potential energy surface encountered by an approaching cation.

For the spherand in the alkali metal cation complexes of **1**, the map plane was defined as the plane passing through the cation in an orientation parallel to, but slightly offset from, the mirror plane of the macrocycle. For the spherand in the complex with $\underline{t}$-$BuNH_3^+$, the map was calculated in the plane where the ammonium hydrogens of the ligand would be located. For visualization of the cation binding position determined from the molecular mechanics optimization (which included calculation of contributions from strain, van der Waals, and hydrogen bonding, as well as Coulombic interactions), the ligands are displayed in their optimized position for each spherand MEP map.

In order to interpret the changes in the ion-spherand interaction energy, E_{IS}, and, in particular, the changes in the molecular electrostatic potential pattern of the spherand that occur upon binding, a set of constrained molecular mechanics optimizations was carried out for the complexes. In these calculations, the structure of the spherand was constrained to its

optimized uncomplexed geometry, while the position of the cation was allowed to optimize within this rigid framework using the protocol decribed in the Molecular Mechanics Section above. Then, the MEP of the constrained spherand was calculated both in the spherand mirror plane and in the plane of the ammonium hydrogens for comparison with the maps described above. As above, however, for visualization of the cation binding position, the ligands are displayed in their optimized positions along with the maps. The CHEM-X[27] "Set Map" facility was used to calculate and display the MEPs. Comparison of the electrostatic component of the ion-spherand interaction energy, $E_{EL}(IS)$, from the constrained and unconstrained optimizations allows quantification of the degree of electrostatic complementarity for the guest presented by the host in its uncomplexed and complexed conformations. Comparison of the MEP patterns of the spherand in its constrained and unconstrained geometries in the complexes provides a way of visualizing the source of the changes in $E_{EL}(IS)$.

RESULTS

Molecular Mechanics Results. Tables I-III give the results of the molecular mechanics energy minimization of **1** and of the cation complexes of **1**. The numbers in parentheses under the Li^+ column represent the results of minimization of the time-averaged molecular dynamics structure of the Li^+-**1** complex. Inspection of Table I shows that, in the complexes, the dihedral angles between adjacent rings of the spherand are smaller than in the uncomplexed spherand. Except for the Na^+ complex and the time-averaged molecular dynamics Li^+ complex, the angles involving fragment A6

are larger than the other inter-ring angles and there is not much variation in the angles with the type of cation being complexed. This indicates that it is the A6 fragment, substituted with methylene groups at positions 2 and 6 of the ring, that gives the spherand the flexibility to accomodate a number of different cations in the binding site. In this sense, then, the spherand is not preorganized to select and discriminately bind only one cation. This will be interpreted in more detail in terms of energy component analysis in the Molecular Dynamics Section below.

Comparison of the two sets of angles for the Li^+ complex shows that the two structures are very different, especially in the orientation of the A6 fragment with respect to the cation. In the first structure, the dihedral angles involving A6 are around 73-80°; in the structure in the second column, the A6 fragment bends in towards the ion to a much greater degree, forming dihedral angles of only 50°. The difference in the structures is seen more clearly in Table II, which gives the distances between the cation and the various spherand oxygens. From the first column of the Li^+ data, it can be seen that the cation is located close to O3, O5, O2, and O4 (of fragments U3, U5, A2, and A4, respectively). The ion is especially close to oxygens O3 and O5 and, consequently, is situated off the C_i symmetry plane of the spherand which passes through fragments U3 and A6. Thus, from this structure another conformation of equivalent energy can be obtained by reflection through the mirror plane of the spherand. In this conformation, the Li^+ ion would be in contact with O1 and O3 (rather than with O3 and O5).

For the Li^+ data in the second column, the ion is found near O1, O5, and O6 in the minimized time-averaged molecular dynamics structure. The difference in the two Li^+ positions can be analyzed in terms the depth of their location within the spherand binding site. Structure **1** shows that fragments U1, U3, U5, and A6 point "up", while A2 and A4 point "down". If a plane is defined by the position of the carbonyl oxygens of U1, U3, and U5, then the Li^+ ion in the first column is found to be -0.50 Å below the plane, whereas the Li^+ in the second column is found 0.25 Å above the plane. This highlights the difference in the structures of the Li^+-**1** complexes, and shows the utility of the molecular dynamics simulation technique for exploring the conformational potential energy surface of the moleculular complex to locate alternative binding positions. (The difference in the two Li^+ complexes will also be seen by a comparison of Figs. 3 and 10 which are discussed in the Molecular Dynamics and Molecular Electrostatic Potential Sections below).

Table II shows that, compared to Li^+ which tends to bind "off-center" in the cavity, the other cations are nearly equidistant from the carbonyl and from the ether oxygens. This must be due to the smaller van der Waals radius of Li^+, compared to the other alkali metal cations, which makes it more difficult for the spherand oxygens to simultaneously contact the Li^+ ion and, thereby satisfy one aspect of the principle of complementarity. The inability of Li^+ to be in simultaneous van der Waals contact with several oxygens may account for the variety of binding positions available to the cation.

Using the definition of a "nested" atom as one which is found below the carbonyl plane and a "perched" atom as one located above the plane, Li^+ (in the first column) and Na^+ are found to be nested within the spherand cavity, whereas the larger ions perch on top. This is in agreement with the preliminary X-ray data reported by Cram and coworkers[5,6] for the complex of 1 with $\underline{t}$-$BuNH_3^+$ and for the complex of a similar macrocycle (with A3 replacing U3) with Cs^+ and Na^+. In these X-ray data, the larger cations perch above the spherand, whereas Na^+ nests within.

Table III summarizes the components of the ion-spherand complexation energy, as calculated from Eqns. (1)-(5), for the molecular mechanics energy minimization of the complexes. The table shows that the spherand reorganization energy, $E_{RE}(S)$, decreases as alkali metal cation size increases. Since Eq. (4) defines the spherand reorganization energy as the energy of the spherand in its complexed conformation relative to the energy in its uncomplexed conformation, a low value for $E_{RE}(S)$ indicates that the spherand undergoes little conformational (and related energetic) change upon complexation. This is also indicated by the relatively small values for $\Delta E_{STR}(S)$, $\Delta E_{VDW}(S)$, and $\Delta E_{EL}(S)$. This result agrees with a comparison of the X-ray structures of 1 and the complex of 1 with $\underline{t}$-$BuNH_3^+$, which indicates that the conformation of the complexed spherand is nearly guest independent[5]. This result is also seen in Table I, in which the dihedral angles between adjacent rings in the Cs^+ and $\underline{t}$-$BuNH_3^+$ complexes are closer to those in the uncomplexed spherand than to those in the Li^+ and Na^+ complexes.

Table III also shows that, for all the complexes, the unfavorable (positive) spherand reorganization energy, $E_{RE}(S)$, is offset by the favorable ion-spherand interaction energy, E_{IS}. E_{IS}, in turn, is dominated by the favorable ion-spherand electrostatic interaction energy, $E_{EL}(IS)$. The trade-off between the spherand reorganization energy and the ion-spherand electrostatic interaction energy results in a favorable complexation energy. Since these trends are also seen in the molecular dynamics simulation results (Table VIII below), further interpretation of the trends is terms of the principles of complementarity and preorganization will be deferred to the Molecular Dynamics Section.

Molecular Dynamics Simulation of the Uncomplexed Spherand. A stereo view of the time-averaged molecular dynamics structure of the uncomplexed spherand is shown in Figure 1. The dihedral angles

INSERT Fig.1

between adjacent fragments of this conformation are listed in Table IV. The data show that these fragments are nearly perpendicular with an average angle of 84.4°. These relatively large angles arise from the electrostatic repulsion of the six spherand oxygens unshielded by a bound cation. Comparison to the molecular mechanics results of Table I indicates that the orientation of the dihedral angles is very similar in the two structures.

Figure 2 contains 15 superimposed structures obtained at 20 ps

INSERT Fig. 2

intervals over the 300 ps of molecular dynamics simulation carried out for the uncomplexed spherand. Examination of this

figure demonstrates that the spherand shows little conformational variation on the time scale of the simulation. Fragment A6 shows more flexibility than the other spherand fragments (except for the rotation of the methoxy groups on fragments A2 and A4). This observation is supported quantitatively by the RMS atomic fluctuation data in Table V. The first column of Table V gives the RMS atomic fluctuations for each of the fragments of the uncomplexed spherand. The largest values, 0.47 and 0.45 Å, are for the A2 and A4 fragments, and are the result of the free rotation of the methoxy groups. Fragment A6 has the next largest RMS atomic fluctuation, 0.39 Å, which is due to "hinge bending" motion of the fragment observed in Fig. 2. The presence of the methylene substituents on A6 allows this extra freedom of motion in this fragment.

Cram and coworkers[8] have shown that the ^1H NMR spectrum of **1** gives a mixture of four conformers, which they interpreted as being due to ring inversion of A6. They also found that addition of $CH_3NH_3ClO_4$ gave a spectrum with two complexes in a 3:1 ratio[8]. From examination of molecular models, they determined that the dominant conformation corresponded to the same orientation of the fragments as in the X-ray structure[5] of **1** complexed with $\underline{t}$-$BuNH_3^+$ and that the subordinate conformation had the A6 ring inverted by about 180^0. However, since the time scale of the ring inversion is longer than the length of the simulation, the molecular dynamics simulation was unable to observe this process.

Molecular Dynamics Simulation of Complexes. Figs. 3-8 present stereo views of the time-averaged structures of the complexes of **1**

INSERT Fig. 3-8

with Li^+, Na^+, K^+, Rb^+, Cs^+, and $\underline{t}$-$BuNH_3^+$, respectively. The position of the alkali metal cation is indicated by the cross-hatched circle; the size of the circle is not related to the van der Waals radius of the ion. The dihedral angles between adjacent fragments of the spherand in these complexes are listed in Table IV. The data show that the inter-fragment dihedral angles are smaller in the complexes than in the uncomplexed spherand. This means that the spherand oxygens are drawn in towards the cation (and towards one another) during the complexation process. This is supported by a comparison of the average oxygen-oxygen distances from the simulations of the complexed and uncomplexed spherand. The angles involving A6 are much smaller in the Li^+ and Na^+ complexes than in the Cs^+ or $\underline{t}$-$BuNH_3^+$ complexes; the other angles show very little variation with the size of cation being complexed. Except for the dihedral angles involving the A6 fragment in the Li^+ complex, these trends agree with the molecular mechanics results of Table I and can be seen qualitatively by inspection of Fig. 3-8. In the spherand complexes with the smaller cations, the increased electrostatic repulsion due to the closer proximity of the spherand oxygens is probably offset by the strong interaction of the oxygens with the cation. The energetics of the complexation process will be discussed in greater detail below.

Table V compares the RMS atomic fluctuations for the spherand fragments in the complexed and uncomplexed structures. The table shows that, in general, due to the organization of the host by the

guest, the RMS fluctuations of the fragments in the complexes are less than in the uncomplexed spherand. In particular, the RMS fluctuations for the atoms of the A2 and A4 fragments decrease from 0.45-0.47 Å in the uncomplexed spherand to around 0.26 Å in the complexes. This result is probably due to lack of free rotation of the methoxy groups once the ion is complexed. The A6 fragment, however, exhibits the same degree of RMS atomic fluctuations in the uncomplexed spherand as in the complexes. This is probably due to the extra degree of flexibility imparted to this fragment by the methylene groups.

Table VI reports the RMS atomic deviations of each of the time-averaged structures of the complexed spherand compared to the time-averaged structure of **1**. The results indicate that the deviations are the smallest for the Cs^+ and $\underline{t}$-$BuNH_3^+$ complexes, indicating that the structure of the spherand in these complexes is most like that of the uncomplexed spherand. This is in agreement with the molecular mechanics results described above and with the preliminary X-ray data[5] for **1** and for the complex of **1** with $\underline{t}$-$BuNH_3^+$. The results of Tables IV-VI imply that the spherand is least conformationally preorganized for complexing the Li^+ ion because it must significantly reorient the A6 fragment in order to provide a complementary binding site for Li^+. This can be seen by a comparison of Fig. 3 to Figs. 1 and 4-8.

Tables VII summarizes the ion-oxygen distances obtained from the molecular dynamics simulation. Except for the differences between the Li^+ complexes noted in the Molecular Mechanics Section above, comparison of the structural data of Tables IV and VII to

that of Tables I and II shows that the corresponding angle and distance quanities obtained with the molecular mechanics and molecular dynamics methods are quite similar for each of the molecular systems. This suggests that, except for the Li^+ complex, each molecular dynamics trajectory evolves in a region of conformational space around the potential energy minimum represented by the initial molecular mechanics conformation. Table VII also shows that the RMS fluctuation of the ion around its average position is, in general, smaller for the other cations than for Li^+. This may indicate that the spherand oxygens are unable to provide the optimal complementary binding site for Li^+ which, according to the principle of complemetarity, should "simultaneously contact and attract"[3] the ion. As a result, the Li^+ ion is allowed to move around in the binding site a bit more than the larger ions.

Inspection of Figs. 3-8 and comparison of the distance of the ion from the plane of the carbonyl oxygens (Table VII) shows that only Na^+ nests in the spherand cavity. In particular, Fig. 3 shows the binding position of Li^+ to be slightly above the plane due to its interaction with O1, O5, and O6 (Table VII). This is in contrast to the molecular mechanics results of Tables II and III, which found only a nested conformation for Li^+ (with Li^+ close to O3, O5, O2, and O4). In contrast, Figs. 4-8 and Table VII show that the larger cations are more equally balanced in their interactions with the carbonyl oxygens than is Li^+.

Finally, Table VII shows that each ammonium hydrogen of $\underline{t}$-$BuNH_3^+$ is, on the average, 1.74 Å from its nearest carbonyl

oxygen. This is due to the fact that the ammonium hydrogens perch tripod fashion on the carbonyl oxygens, in contrast to the orientation of the centrally-bound alkali metal cations. This orientation of the ligand is found in the X-ray structure[5].

Table VIII summarizes the components of the ion-spherand complexation energy for the molecular dynamics simulations. The table shows the same trends as the molecular mechanics results in Table III. The spherand reorganization energy is positive and it decreases as alkali metal cation size increases. The strain, van der Waals, and electrostatic components of the spherand reorganization energy are given in rows 3-5 of the table. Since the SHAKE algorithm was used, there is no bond stretching contribution to the strain energy of the spherand (or $\underline{t}$-$BuNH_3^+$). The dominant contributor to $F_{RE}(S)$ is the positive electrostatic energy which results principally from the decreased oxygen-oxygen distances in the structure of the complexed spherand compared to those in the uncomplexed spherand. This is a result of the decrease in the average dihedral angles between adjacent rings (Table IV) as the oxygens are drawn in to provide an optimal, complementary binding site which "simultaneously contacts and attracts" the alkali metal cations. This electrostatic component of $E_{RE}(S)$ decreases with increased alkali metal cation size and oxygen-oxygen distances, while the average dihedral angles between adjacent fragments increase.

Except for the slightly positive energy calculated for the Li^+ complex, the strain component generally forms a favorable contribution to $E_{RE}(S)$. The reorganization energy of the spherand

is thus kept lower because the increased oxygen-oxygen electrostatic repulsion incurred upon complexation is somewhat offset by a decrease in the strain energy in the spherand.

Table VIII also gives the energy of $\underline{t}$-$BuNH_3^+$ in the ion-spherand complex. Compared to the energy of the uncomplexed ion, -21.5 Kcal/mol, this gives an ligand reorganiztion energy of 1.1 Kcal/mol. This is consistent with the X-ray data[5] which indicates that the $\underline{t}$-$BuNH_3^+$ cation perches on top of the macrocycle and is unlikely to undergo a large conformational change upon binding.

Table VIII shows that, in agreement with the molecular mechanics results of Table III, the unfavorable spherand reorganization energy, $E_{RE}(S)$, is offset by the favorable electrostatic component, $E_{EL}(IS)$, of the ion-spherand interaction energy, resulting in a favorable complexation energy. Even though the spherand reorganization energy becomes increasingly positive with decreasing ionic size, the ion-spherand interaction energy becomes even more negative (i.e., favorable) so that the reorganization energy of the spherand is generally only 10%-20% of the magnitude of E_{IS}, regardless of the degree of spherand distortion.

E_{IS} ?
COMM
SYMBO

Molecular Mechanics Results for Constrained Optimization of Complexes. Both the molecular mechanics results (Table III) and molecular dynamics results (Table VIII) indicate that it is the electrostatic component of the ion-spherand interaction energy, $E_{EL}(IS)$, which determines the overall favorable complexation energy. This quantity can be analyzed in terms of the principle of

complementarity as follows. Table IX compares the value of $E_{EL}(IS)$ for the complexes in which the spherand geometry was allowed to optimize versus those in which it was constrained to its uncomplexed conformation. The difference in the two values quantifies the degree of electrostatic complementarity presented to each cation by the spherand in its uncomplexed conformation. A large difference in $E_{EL}(IS)$ indicates that the structure of the uncomplexed spherand does not provide the optimally attractive binding site for the cation and that some degree of spherand reorganization should be required for binding. Table IX shows that the largest differences in $E_{EL}(IS)$ are for the smaller cations, Li^+ and Na^+. The differences decrease with increasing alkali metal cation size and are smallest for $\underline{t}$-$BuNH_3^+$. These differences correlate with the trends in spherand reorganization energy noted in Tables III and VIII: the smaller cations must expend a larger reorganization energy in order to optimally bind the cation.

The differences in $E_{EL}(IS)$ quantified in Table IX are visualized through the molecular electrostatic potential maps discussed below.

Molecular Electrostatic Potential Patterns. Fig. 9 repre-

INSERT Fig.9

sents the molecular electrostatic potential pattern which corresponds to the constrained spherand calculation of Table IX. The figure is a plot of $E_{EL}(IS)$ calculated for the interaction of the spherand with a unit positive point charge located at grid points throughout the mirror plane of the uncomplexed spherand. In

addition, the binding position (indicated by atom label) of each alkali metal cation determined from the constrained molecular mechanics optimization is indicated on the figure. The figure is a representation of where the cations would bind if the spherand were constrained to its uncomplexed conformation. Examination of the map shows that the three most negative regions of potential energy (-160 Kcal/mol) are located close to the O3 atom of fragment U3 on the right side of the figure, as well as near the O6 and ring regions of fragment A6 on the left. In the region of the spherand where Li^+, Na^+, and K^+ ions bind, the potential energy surface is around -40 to -80 Kcal/mol; above this region, where Rb^+ and Cs^+ bind, the surface is around -40 Kcal/mol.

Figs. 10-14 give MEP maps of the spherand from the

INSERT Figs. 10-14

unconstrained optimization of the alkali metal cation complexes. Comparison of these figures to Fig. 9 shows that in the unconstrained complexes, the value of the MEP energy at the ion binding site is much more negative than in Fig. 9. For example, Li^+, Na^+, and K^+ bind in regions where the potential is around -120 to -160 Kcal/mole (Fig. 10-11), compared -40 to -80 Kcal/mol in the constrained spherand (Fig. 9). Rb^+, and Cs^+ bind in regions where the MEP is closer to -80 Kcal/mol (Fig. 12-14), compared to -40 Kcal/mol (Fig. 9). The figures show that the spherand presents a much more favorable binding site for the alkali metal cations when it adopts its complexed conformation. In particular, comparison of Figs. 9 and 10 shows that the largest differences in the MEP at the position of ion binding, compared to the MEP of the uncomplexed

conformation of the spherand, occur for the spherand in its complex with Li^+. The figures are a means of interpreting the results of Table IX, which show that the largest difference in E_{EL}(IS), -65.4 Kcal/mol, is for the smallest cation, Li^+. This indicates that, as a result of the conformational reorganization allowed during the unconstrained optimization of the complex, the spherand is able to present a more attractive binding site to the smaller alkali metal cations. This indicates the interplay between the principles of complementarity and preorganization and underscores the fact that the molecular architecture of the spherand is the least preorganized for binding the Li^+ cation. This is in agreement with the measurement of binding free energies for extraction of the picrate salts of the guests from D_2O into a solution of **1** in $CDCl_3$, which shows Li^+ to have the lowest value in the series[6].

Inspection of Figs. 9-14 also shows that the MEP pattern determines the directionality of approach of the ion to the binding site. The contour level at 0 Kcal/mol slices through the spherand, indicating that more positive regions are to be found at the bottom of the figure; the attractive, negative regions are at the top, near the A6 methoxy oxygen and the cyclic urea carbonyl oxygen atoms. An approaching cation would, therefore, be electrostatically steered towards this latter, more favorable direction of approach.

Comparison of the nested location of Li^+ in the molecular mechanics structure of Fig. 10 to its position in the time-averaged molecular dynamics structure of Fig. 3 visually indicates the

differences in the ion binding position noted in the discussion of Tables II and VII.

Figure 15 contains the MEP of the spherand in its

INSERT Fig. 15

conformation in the constrained optimization of **1** with $\underline{t}$-$BuNH_3^+$. The map is calculated in the plane of the ammonium hydrogens and the ligand is shown in its binding orientation with only two ammonium hydrogens associated with the carbonyl oxygens of U3 and U5. The inability of the spherand to adjust its conformation to accomodate the ligand probably accounts for the two-point binding shown in the figure. The MEP contour levels at the ammonium hydrogen positions are (-80 Kcal/mol). From Table IX, it can be seen that the average electrostatic interaction energy of the constrained spherand with each ammonium hydrogen is -22.1 Kcal/mol.

Fig. 16 contains the MEP of the spherand in its

INSERT Fig. 16

conformation in the unconstrained optimization of the complex of **1** with $\underline{t}$-$BuNH_3^+$. The map is calculated in the plane of the ammonium hydrogens and the ligand is displayed in its binding orientation with each of the ammonium hydrogens bonded to a cyclic urea oxygen. The regions of minimum electrostatic potential energy (around -160 Kcal/mol) are found near each of the three carbonyl oxygens (O1, O3, and O5 of fragments U1, U3, and U5, respectively) and the methoxy oxygen (O6) of A6. Each of the ammonium hydrogens is close to a minima at a carbonyl oxygen. From Table IX, the average electrostatic interaction energy of the spherand with each ammonium hydrogen is calculated to be -36.5 Kcal/mol. The difference

compared to the constrained spherand calculation is thus only -14.4 Kcal/mol per ammonium hydrogen atom. The spherand, therefore, appears to be well-designed for the tripod-like perching of the $\underline{t}$-$BuNH_3^+$ cation.

In summary, it is seen that very significant changes in the spherand electrostatic potential energy favorable to binding these cations are thus induced upon complexation. This occurs as the result of a small conformational change in the spherand in which the spherand oxygens are drawn towards the centrally bound ion, resulting in a significant enhancement of the molecular electrostatic potential pattern around the oxygen atoms. Thus, although the uncomplexed spherand presents a negative electrostatic potential pattern which is complementary in sign to that of the cation, the magnitude of the electrostatic potential of the uncomplexed spherand is not optimal for binding the alkali metal ions. Thus, the significant increase in the magnitude of the electrostatic potential in the ion binding region of the spherand when it adopts its complexed conformation indicates that the resulting enhancement of the intermolecular electrostatic interaction energy is a major component of the total complexation energy.

CONCLUSIONS

Molecular mechanics calculations and molecular dynamics simulations have been carried out for the complexes of **1** with alkali metal cations and a $\underline{t}$-$BuNH_3^+$ ligand in order to quantify and interpret the interrelated principles of preorganization and

complementarity. The results show that it is the flexibility of fragment A6 which allows **1** to provide a binding site which is complementary to all the ligands. Analysis of the components of the complexation energy shows that the larger reorganization energy expended by the spherand in order to complex the smaller cations is offset by the overwhelmingly favorable intermolecular electrostatic interaction energy. Spherand **1** is, therefore, not a discriminant binder of alkali metal cations. Because of this ability to complex all the alkali metal cations fairly well, Cram and coworkers[8] have identified **1** as one of the best neutral extraction agents for cations. More rigid spherand binding sites have been designed by Cram and coworkers[3] to complex only Li^+ and Na^+, while rejecting K^+, Ca^{+2}, and Mg^{+2}.

As noted in the Introduction, however, one aspect of preorganization has not been addressed in this paper---the degree of reorganization of the solvent molecules that occurs upon complexation. Since the calculated complexation energy decreases with alkali metal cation size, whereas the binding free energy goes through a maximum value for the K^+ ion[5,6], it is clear that the entropic contribution must be considered in a complete discussion of the energetics of complexation. In addition, it is possible that the strength of the electrostatic interactions noted here will be damped by the inclusion of solvent in the calculation. These points will be addressed in a future publication.

ACKNOWLEDGEMENTS

This work was supported by grants to C.A.V. from The New Jersey Commission on Science and Technology, the Office of Naval

Research, and the Ciba-Geigy, Schering-Plough, Hoffmann LaRoche, and BOC Corporations. C.A.V. wishes to acknowledge a generous grant of computer time from New Jersey Institute of Technology.

REFERENCES

(1) Trueblood, K.N.; Knobler, C.B.; Maverick, E.; Helgeson, R.C.; Brown, S.B.; Cram, D.J. J. Am. Chem. Soc., **1981**, 103, 5594.

(2) Cram, D.J.; Lein, G.M.; Kaneda, T.; Helgeson, R.C.; Knobler, C.B.; Maverick, E.; Trueblood, K.N. J. Am. Chem. Soc., **1981**, 103, 6228.

(3) Cram, D.J.; Kaneda, T.; Helgeson, R.C.; Brown, S.B.; Knobler, C.B.; Maverick, E.; Trueblood, K.N. J. Am. Chem. Soc., **1985**, 107, 3645-3657.

(4) Cram, D.J.; Lein, G.M. J. Am. Chem. Soc., **1985**, 107, 3657-3668.

(5) Cram, D.J.; Dicker, I.B.; Knobler, C.B.; Trueblood, K.N. J. Am. Chem. Soc., **1982**, 104, 6828-6830.

(6) Cram, D.J.; Dicker, I.B.; Lauer, M.; Knobler, C.B.; Trueblood, K.N. J. Am. Chem. Soc., **1984**, 106, 7150-7167.

(7) Cram, D.J.; Katz, H.E. J. Amer. Chem. Soc., **1983**, 105, 135-137.

(8) Cram, D.J.; Katz, H.E.; Dicker, I.B. J. Amer. Chem. Soc. **1984**, 106, 4987-5000.

(9) Cram, D.J.; Lam, P.Y.-S.; Ho, S.P. J. Amer. Chem. Soc., **1986**, 108, 839-841.

(10) Venanzi, C.A.; Bunce, J.D. Enzyme, **1986**, 36, 79-92.

(11) Venanzi, C.A.; Bunce, J.D. Ann. N. Y. Acad. Sci. **1986**, 471, 318-320.

(12) Venanzi, C.A.; Bunce, J.D. Int. J. of Quantum Chem., **1986**, 12, 69-87.

(13) Venanzi, C.A. In "Environmental Influences and Recognition in Enzyme Chemistry", Liebman J.F. and Greenberg, A., Eds.; VCH, New York, 1988, pp. 251-279.

(14) Venanzi, C.A.; Namboodiri, K. Anal. Chim. Acta, **1988**, 210, 151-162.

(15) Kollman, P.A.; Wipff, G.; Singh, U.C. J. Am. Chem. Soc. **1985**, 107, 2212-2219.

(16) Gehin, D.; Kollman, P.A.; Wipff, G.A. J. Am. Chem. Soc. **1989**, 111, 3011-3023.

(17) Artz, S.P.; Cram, D.J. J. Am. Chem. Soc. **1984**, 106, 2160-2170.

(18) Singh, U.C.; Weiner, P.K.; Caldwell, J.W.; Kollman, P.A., University of California at San Francisco, 1986.

(19) Weiner, S.J.; Kollman, P.A.; Case, D.A.; Singh, U.C.; Ghio, C.; Alagona, G.; Profeta, S.; Weiner, P. J. Amer. Chem. Soc., **1984**, 106, 765-784.

(20) Singh, U.C.; Kollman, P.A. J. Comput. Chem. **1984**, 5, 129-145.

(21) Singh, U.C.; Kollman, P. Quantum Chemistry Exchange Program Bull., **1982**, 2, 17.

(22) Cox, S.R.; Williams, D.E. J. Comp. Chem., **1981**, 2, 304-323.

(23) Grootenhuis, P.D.J.; Kollman, P.A. J. Am. Chem. Soc., **1989**, 111, 2152-2158.

(24) Trueblood, K.N., personal communication.

(25) Berendsen, H.J.C.; Postma, J.P.M.; van Gunsteren, W.F.; DiNola, A.; Haak, J.R. J. Chem. Phys., **1984**, 81, 3684-3690.

(26) Van Gunsteren, W.F.; Berendsen, H.J.C. Molecular Phys., **1977**, 34, 1311-1327.

(27) Chem-X, developed and distributed by Chemical Design, Ltd., Oxford, England.

TABLE I. Dihedral Angles[a] Between Adjacent Rings. Molecular Mechanics Results.

	Uncomplexed	Complexes					
	Spherand	Li^+	Na^+	K^+	Rb^+	Cs^+	$\underline{t}$-$BuNH_3^+$
U1/A2	76.2	54.8	(57.5)[b]	56.9	61.8	63.6	66.0	61.5
A2/U3	76.2	49.1	(61.8)	55.5	60.0	62.1	64.3	60.1
U3/A4	76.6	53.7	(62.0)	55.4	58.8	60.4	62.4	59.0
A4/U5	76.3	53.3	(57.7)	57.1	62.1	63.3	65.2	61.3
U5/A6	85.8	72.7	(50.3)	54.8	64.7	72.0	78.6	78.7
A6/U1	85.5	79.7	(50.8)	56.1	67.5	75.0	81.6	80.9

a. Angles in degrees.

b. Numbers in parentheses are from molecular mechanics minimization of the time-averaged molecular dynamics structure.

TABLE II. Ion-Spherand Oxygen Distances.[a] Molecular Mechanics Results.

	Li^+		Na^+	K^+	Rb^+	Cs^+	$\underline{t}$-$BuNH_3^+$
Carbonyl Oxygens							
O1	3.04	(1.85)[b]	2.32	2.62	2.78	3.00	1.71[c]
O3	1.86	(3.21)	2.34	2.63	2.79	3.04	1.73
O5	1.92	(1.84)	2.29	2.60	2.76	2.98	1.71
Average	2.27	2.30	2.32	2.62	2.78	3.01	1.72
Ether Oxygens							
O2	2.08	(3.20)[b]	2.58	3.01	3.44	4.00	2.64[c]
O4	2.00	(3.22)	2.59	2.98	3.39	3.95	2.60
O6	3.97	(1.94)	2.69	2.82	3.00	3.26	2.87
Average	2.68	(2.79)	2.62	2.94	3.28	3.74	2.70
Distance[e] from Plane of Carbonyl Oxygen Atoms	-0.50	(0.25)	-0.11	0.28	0.74	1.30	0.29[d]

a. Distances in Angstroms.

b. Numbers in parentheses are from molecular mechanics minimization of the time-averaged molecular dynamics structure.

c. Numbers in this column give the distance of the cyclic urea oxygen to the nearest ammonium hydrogen atom.

d. Average distance of the three ammonium hydrogens from the plane.

e. Perpendicular distance from the plane defined by the carbonyl oxygens O1, O3, and O5. A positive value indicates a position above the plane (in the direction of O6); a negative value indicates a position below the plane (in the direction of O2 and O4).

TABLE III. Ion-Spherand Complexation Energetics[a]. Molecular Mechanics Results.

	Complexes						
	Li^+		Na^+	K^+	Rb^+	Cs^+	$\underline{t}$-$BuNH_3^+$
E_S[b]	-89.8	(-85.3)[c]	-92.2	-102.4	-105.0	-107.6	-105.2
$E_{RE}(S)$[d]	26.8	(31.3)	24.5	14.2	11.6	9.1	11.4
$\Delta E_{STR}(S)$	-3.3	(5.0)	-2.4	-4.2	-4.4	-4.6	-4.8
$\Delta E_{VDW}(S)$	9.0	(1.8)	3.9	1.9	1.8	1.7	2.1
$\Delta E_{EL}(S)$	21.1	(24.4)	22.9	16.4	14.0	11.9	14.0
E_I[e]	-----	------	-----	-----	-----	-----	-21.4
$E_{RE}(I)$	-----	------	-----	-----	-----	-----	0.1
$E_{VDW}(IS)$	3.6	(4.8)	4.7	7.6	6.9	5.0	-4.2
$E_{EL}(IS)$	-131.4	(-136.5)	-117.8	-93.9	-82.9	-70.8	-89.1
$E_{HB}(IS)$	------	------	------	-----	----	-----	-0.6
E_{IS}	-127.8	(-131.7)	-113.1	-86.4	-76.0	-65.8	-94.0
E_T	-217.6	(-217.0)	-205.3	-188.8	-181.0	-173.4	-199.2
E_C	-101.0	(-100.4)	-88.7	-72.1	-64.4	-56.8	-82.4

a. Energy in Kcal/mole. See text for definition of energy terms.

b. For the uncomplexed spherand, $E_{S'}$ = -116.6 Kcal/mol. $E_{S'}$ PRIME SYMBOL

c. Numbers in parentheses refer to molecular mechanics minimization of the time-averaged molecular dynamics structure.

d. There is no hydrogen bonding contribution to the energy of the uncomplexed or complexed spherand, and, therefore, no hydrogen bonding contribution to the reorganization energy.

e. For the uncomplexed $\underline{t}$-$BuNH_3$, $E_{I'}$ = -21.5 Kcal/mol. $E_{I'}$ PRIME SYMBOL

TABLE IV. Average Dihedral Angles[a] Between Adjacent Rings. Molecular Dynamics Results.

	Uncomplexed	Complexes					
	Spherand	Li^+	Na^+	K^+	Rb^+	Cs^+	$\underline{t}$-$BuNH_3^+$
U1/A2	80.1	59.3	58.9	64.4	66.3	67.8	63.5
A2/U3	88.0	63.5	57.4	62.2	64.8	67.1	62.6
U3/A4	88.2	63.0	57.1	62.2	64.6	67.2	64.3
A4/U5	79.2	58.9	58.7	64.3	66.2	67.8	64.9
U5/A6	85.3	51.8	57.8	68.2	75.3	80.2	77.8
A6/U1	85.3	51.6	57.6	68.2	74.8	79.9	78.8

a. Angles in degrees.

TABLE V. RMS Atomic Fluctuations[a] of Spherand.

	Uncomplexed Spherand	Complexes					
		Li^+	Na^+	K^+	Rb^+	Cs^+	$\underline{t}$-$BuNH_3^+$
U1	0.30	0.23	0.19	0.20	0.22	0.22	0.23
A2	0.46	0.26	0.20	0.22	0.26	0.26	0.28
U3	0.28	0.18	0.14	0.16	0.19	0.18	0.18
A4	0.45	0.26	0.20	0.22	0.26	0.26	0.25
U5	0.30	0.22	0.20	0.19	0.22	0.22	0.22
A6	0.39	0.34	0.43	0.41	0.44	0.39	0.42
U1-U5[b]	0.37	0.24	0.19	0.20	0.24	0.23	0.24
U1-A6[c]	0.38	0.26	0.25	0.25	0.28	0.27	0.28
Ion	----	0.27	0.17	0.21	0.26	0.21	0.29

a. In Angstroms.

b. Average of fluctuations for all the atoms in fragments U1, A2, U3, A4 and U5.

c. Average of fluctuations for all the atoms in fragments U1, A2, U3, A4, U5 and A6.

TABLE VI. RMS Atomic Deviations[a] of Time-Averaged Complexed Spherand Structures from Time-Averaged Uncomplexed Spherand Structure.

	Complexes					
	Li^+	Na^+	K^+	Rb^+	Cs^+	$\underline{t}$-$BuNH_3^+$
U1	0.53	0.34	0.16	0.12	0.10	0.17
A2	0.50	0.53	0.53	0.49	0.46	0.49
U3	0.58	0.71	0.59	0.53	0.49	0.53
A4	0.46	0.51	0.52	0.48	0.43	0.42
U5	0.52	0.32	0.16	0.12	0.10	0.08
A6	2.04	1.63	1.04	0.78	0.71	0.75
U1-U5[b]	0.52	0.50	0.44	0.40	0.36	0.38
U1-A6[c]	0.99	0.83	0.59	0.49	0.45	0.47

a. In Angstroms.

b. RMS deviation calculated for all the atoms in fragments U1, A2, U3, A4 and U5.

c. RMS deviation calculated for all the atoms in fragments U1, A2, U3, A4, U5 and A6.

TABLE VII. Ion-Spherand Oxygen Distances[a]. Molecular Dynamics Results.

	Li^+	Na^+	K^+	Rb^+	Cs^+	$\underline{t}$-$BuNH_3^+$
Carbonyl Oxygens						
O1	1.88	2.31	2.62	2.79	3.04	1.73[b]
O3	3.16	2.37	2.65	2.84	3.11	1.75
O5	1.87	2.31	2.62	2.79	3.03	1.73
Average	2.30	2.33	2.63	2.81	3.06	1.74
RMS Fluctuation	0.20	0.07	0.06	0.09	0.10	0.05
Ether Oxygens						
O2	3.19	2.65	3.12	3.58	4.16	3.27[c]
O4	3.77	3.38	3.72	4.03	4.44	3.31
O6	2.03	2.74	2.85	3.05	3.29	3.23
Average	3.00	2.92	3.23	3.55	3.96	3.27
RMS Fluctuation	0.26	0.19	0.16	0.22	0.19	0.22
Distance[d] from Plane of Carbonyl Oxygen Atoms	0.19	-0.10	+0.33	+0.85	+1.43	+0.40[c]

a. Average distance (in Angstroms) from 300 ps of simulation.

b. Distance of the cyclic urea oxygen to the nearest ammonium hydrogen atom.

c. Average distance of the three ammonium hydrogens from the plane.

d. Perpendicular distance from the plane defined by the carbonyl oxygens O1, O3, and O5. A positive value indicates a position above the plane (in the direction of O6); a negative value indicates a position below the plane in the direction of O2 and O4).

TABLE VIII. Ion-Spherand Complexation Energetics[a]. Molecular Dynamics Results.

	Complexes					
	Li^+	Na^+	K^+	Rb^+	Cs^+	$\underline{t}$-$BuNH_3^+$
E_S[b]	-73.6	-82.8	-92.2	-92.7	-96.8	-90.9
$E_{RE}(S)$[c]	30.1	20.9	11.5	11.0	6.9	12.8
$\Delta E_{STR}(S)$	1.3	-7.6	-8.9	-7.0	-9.2	-6.3
$\Delta E_{VDW}(S)$	1.7	3.2	1.0	1.1	0.9	1.7
$\Delta E_{EL}(S)$	27.1	25.2	19.3	16.9	15.1	17.3
E_I[d]	------	-----	-----	-----	-----	-20.4
$E_{RE}(I)$	-----	-----	-----	-----	----	1.1
$E_{VDW}(IS)$	4.4	4.9	7.5	6.6	4.4	-3.9
$E_{EL}(IS)$	-134.5	-115.7	-92.3	-80.5	-69.0	-87.8
$E_{HB}(IS)$	------	------	-----	----	-----	-0.7
E_{IS}	-130.1	-110.8	-84.8	-73.9	-64.6	-92.4
E_T	-203.7	-193.6	-177.0	-166.6	-161.4	-203.8
E_C	-100.1	-89.9	-73.3	-62.9	-57.7	-80.7

a. Energy in Kcal/mole. See text for definition of energy terms.

b. For the uncomplexed spherand, $E_{S'}$ = -103.7 kcal/mol.

c. There is no hydrogen bonding contribution to the energy of the uncomplexed or complexed spherand, and, therefore, no hydrogen bonding contribution to the reorganization energy.

d. For the uncomplexed $\underline{t}$-$BuNH_3$, $E_{I'}$ = -21.5 Kcal/mol.

$E_{S'}$ PRIME SYMBOL

$E_{I'}$ PRIME SYMBOL

TABLE IX. Comparison of the Electrostatic Component, $E_{EL}(IS)$, of the Ion-Spherand Interaction Energy[a] for Constrained Versus Unconstrained Molecular Mechanics Optimization of Ion Position.

	Unconstrained Spherand[b]	Constrained Spherand[c]	Difference
Li^+	-131.4	-66.0	-65.4
Na^+	-117.8	-58.3	-59.5
K^+	-93.9	-56.0	-37.9
Rb^+	-82.9	-44.6	-38.3
Cs^+	-70.9	-38.6	-32.3
t-BuNH3$^+$ [d]	-36.5	-22.1	-14.4

a. Energy in Kcal/mol.

b. Both ion and spherand coordinates were optimized (Table III).

c. Ion position was optimized while spherand coordinates were constrained to optimized uncomplexed conformation.

d. Average for the three ammonium hydrogens.

LEGEND TO FIGURES

Fig. 1. Time-averaged molecular dynamics structure of **1** from 300 ps of simulation. In Figs. 1-14, the spherand is shown from a side view with fragment A6 on the left of the figure and fragment U3 on the right. In these figures, O6, O1, O3, and O5 are shown pointing up towards the top of the figure; O2 and O4 point down towards the bottom of the figure.

Fig. 2. Superposition of 15 conformations of **1** taken at 20 ps intervals from the simulation of the uncomplexed spherand.

Fig. 3. Time-averaged structure of the complex of **1** with Li^+. The position of the ion is shown by a cross-hatched circle. Fragment A6 is on the left of the figure with O6 pointing towards the ion. The ion is shown close to the O1 and O5 oxygens of fragments U1 and U5.

Fig. 4. Time-averaged structure of the complex of **1** with Na^+. The position of the ion is shown by a cross-hatched circle. Fragment A6 is on the left of the figure with O6 pointing towards the ion. The ion is shown nested in the binding site, close to the O1, O3, and O5 oxygens of fragments U1, U3, and U5.

Fig. 5. Time-averaged structure of the complex of **1** with K^+. The position of the ion is shown by a cross-hatched circle. Fragment A6 is on the left of the figure with O6 pointing towards the ion. The ion is shown perched above the binding site, close to the O1, O3, and O5 oxygens of fragments U1, U3, and U5.

Fig. 6. Time-averaged structure of the complex of 1 with Rb^+. The position of the ion is shown by a cross-hatched circle. Fragment A6 is on the left of the figure with O6 pointing towards the ion. The ion is shown perched above the binding site.

Fig. 7. Time-averaged structure of the complex of 1 with Cs^+. The position of the ion is shown by a cross-hatched circle. Fragment A6 is on the left of the figure with O6 pointing towards the ion. The ion is shown perched above the binding site.

Fig. 8. Time-averaged structure of the complex of 1 with $\underline{t}$-$BuNH_3^+$. The ligand is shown with the ammonium hydrogens located near the cyclic urea oxygens of fragments U1, U3, and U5. The ligand is perched above the binding site.

Fig. 9. The molecular electrostatic potential pattern of 1 in its uncomplexed conformation. Contour levels are shown at 0, -40, -80, -120, and -160 Kcal/mol. The positions of the alkali metal cations from the constrained molecular mechanics optimizations of the complexes are indicated by atom labels.

Fig. 10. The molecular electrostatic potential pattern of 1 in its conformation in the complex with Li^+. Contour levels are the same as in Fig. 9. The nested position of Li^+ from the unconstrained molecular mechanics optimization of the complex is indicated by atom label.

Fig. 11. The molecular electrostatic potential pattern of 1 in its conformation in the complex with Na^+. Contour levels are the same as in Fig. 9. The nested position of Na^+ from the unconstrained molecular mechanics optimization of the complex is indicated by atom label.

Fig. 12. The molecular electrostatic potential pattern of 1 in its conformation in the complex with K^+. Contour levels are the same as in Fig. 9. The position of K^+ from the unconstrained molecular mechanics optimization of the complex is indicated by atom label.

Fig. 13. The molecular electrostatic potential pattern of 1 in its conformation in the complex with Rb^+. Contour levels are the same as in Fig. 9. The perched position of Rb^+ from the unconstrained molecular mechanics optimization of the complex is indicated by atom label.

Fig. 14. The molecular electrostatic potential pattern of 1 in its conformation in the complex with Cs^+. Contour levels are the same as in Fig. 9. The perched position of Cs^+ from the unconstrained molecular mechanics optimization of the complex is indicated by atom label.

Fig. 15. The molecular electrostatic potential pattern of 1 in its conformation in the complex with $\underline{t}$-$BuNH_3^+$. Contour levels are the same as in Fig. 9. The spherand is shown in a top view with fragment A6 at the bottom of the figure and fragment U3 at the top. The ligand is shown in its position from the constrained molecular mechanics optimization of the complex. The ammonium hydrogens point towards O1, O3, and O5.

Fig. 16. The molecular electrostatic potential pattern of 1 in its conformation in the complex with $\underline{t}$-$BuNH_3^+$. Contour levels are the same as in Fig. 9. The spherand is shown in a top view with fragment A6 at the top of the figure and fragment U3 at the bottom. The ligand is shown in its position from the unconstrained

molecular mechanics optimization of the complex. The ammonium hydrogens point towards O1, O3, and O5.

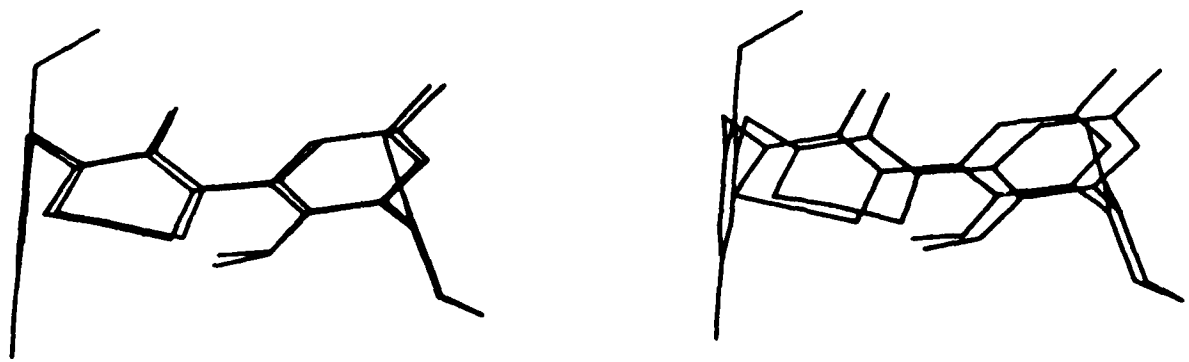

Fig. 1

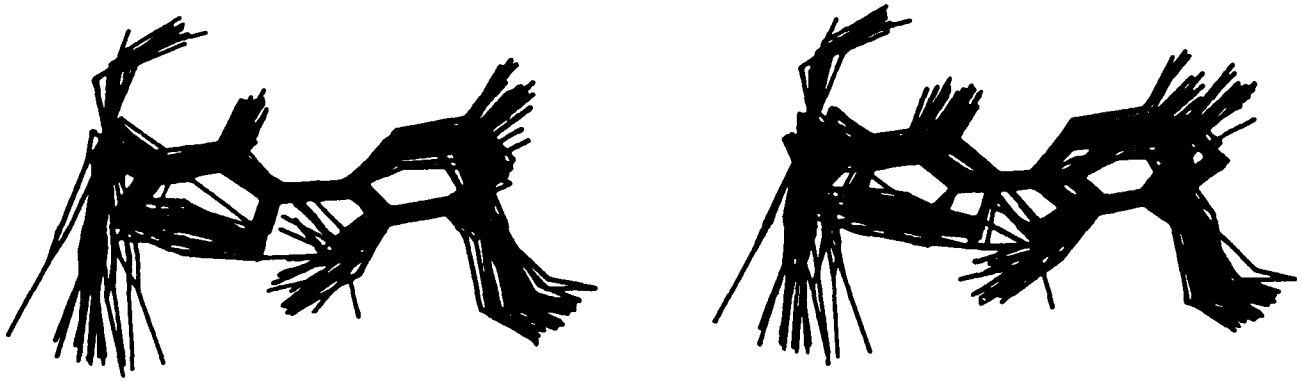

Fig. 2

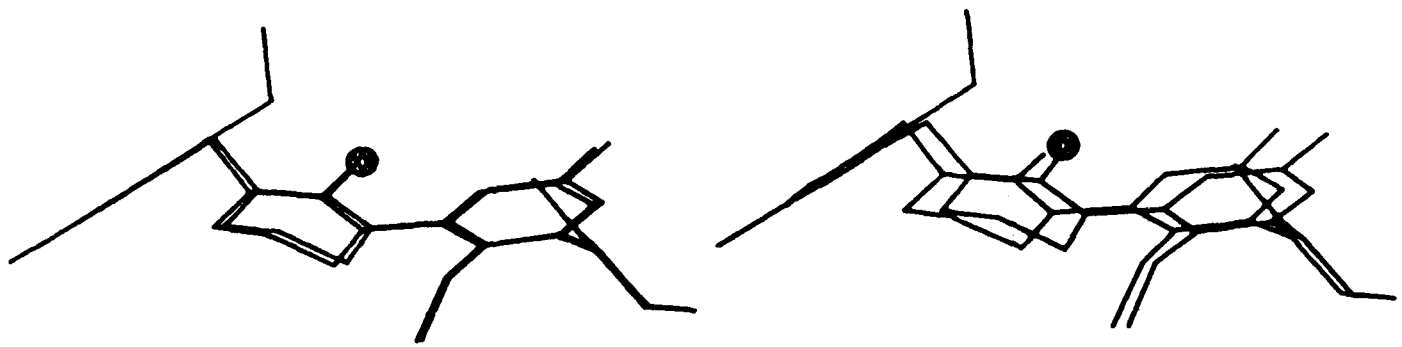

Fig. 3

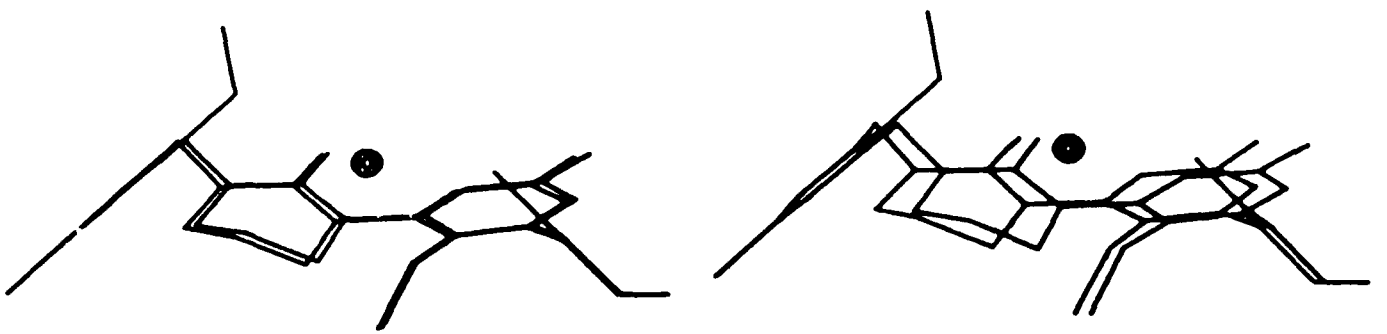

Fig. 4

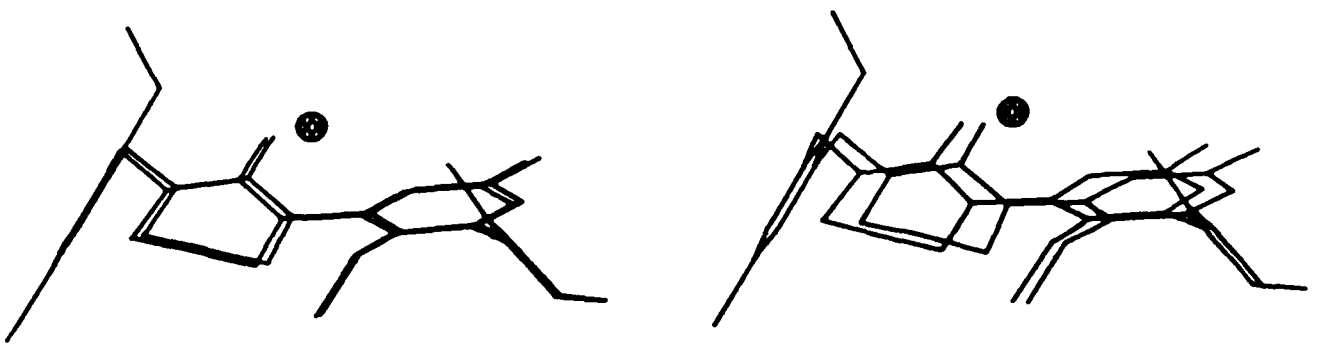

Fig. 5

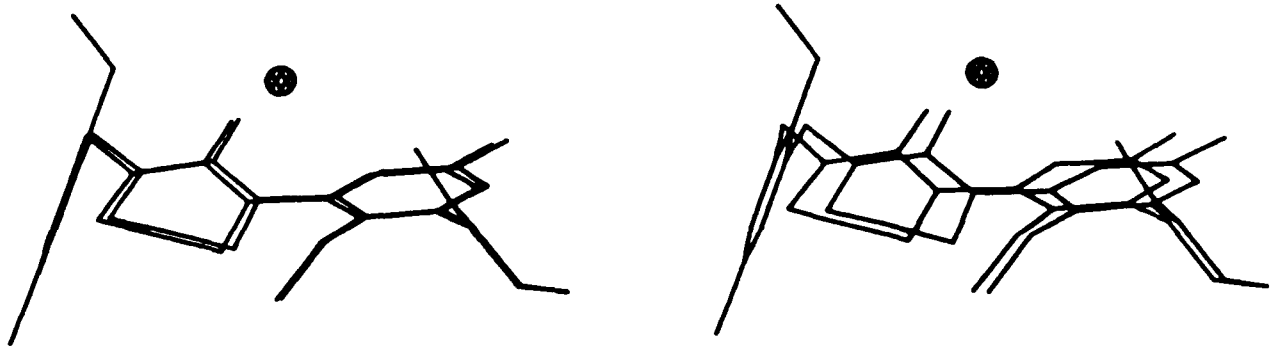

Fig. 6

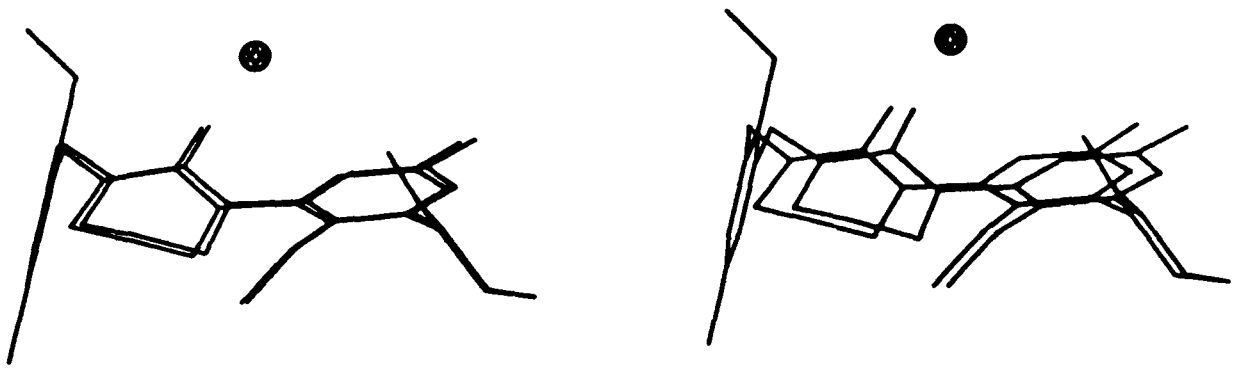

Fig. 7

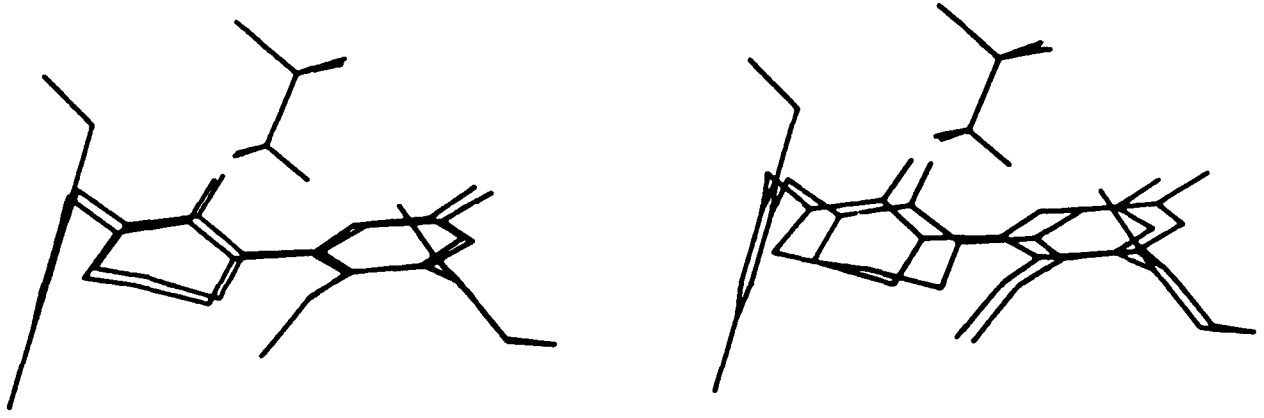

Fig. 8

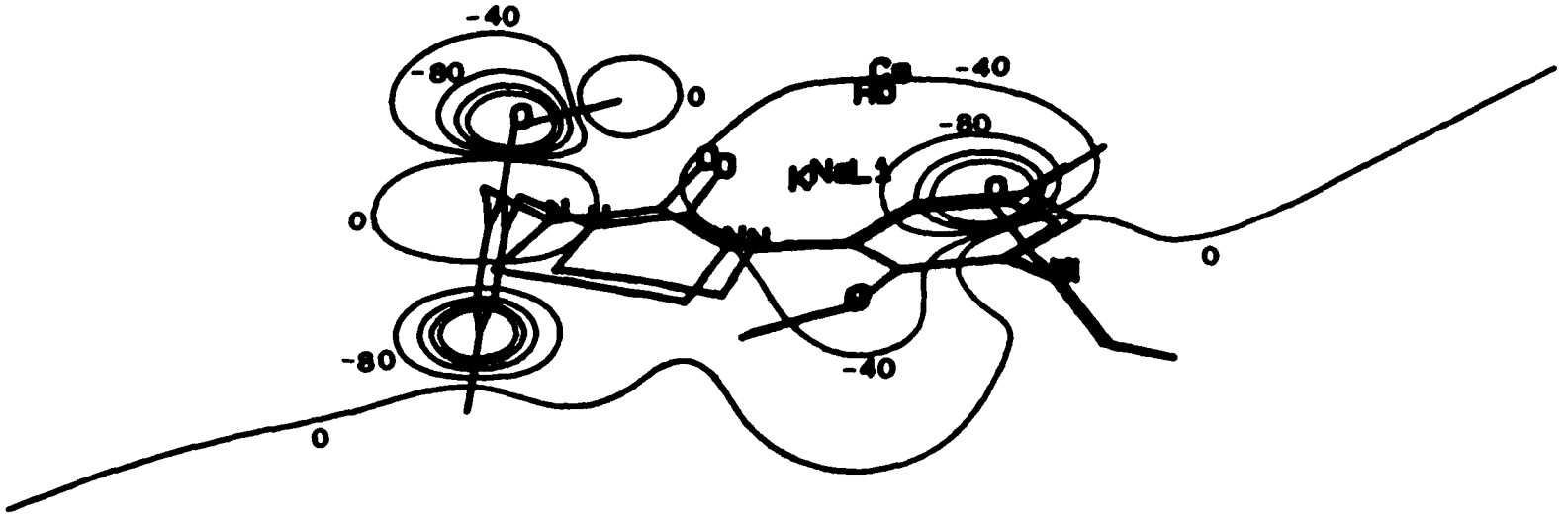

Fig. 9

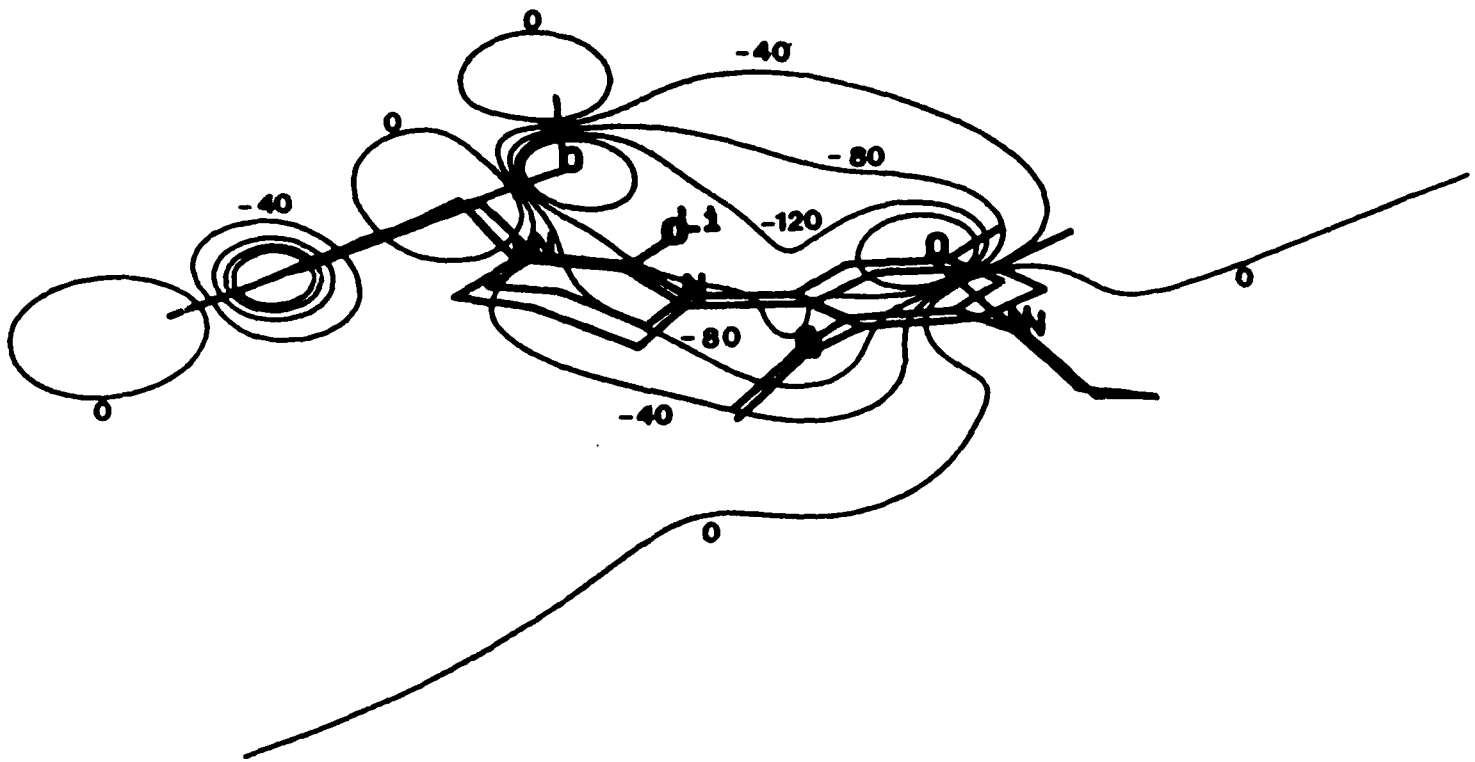

Fig. 10

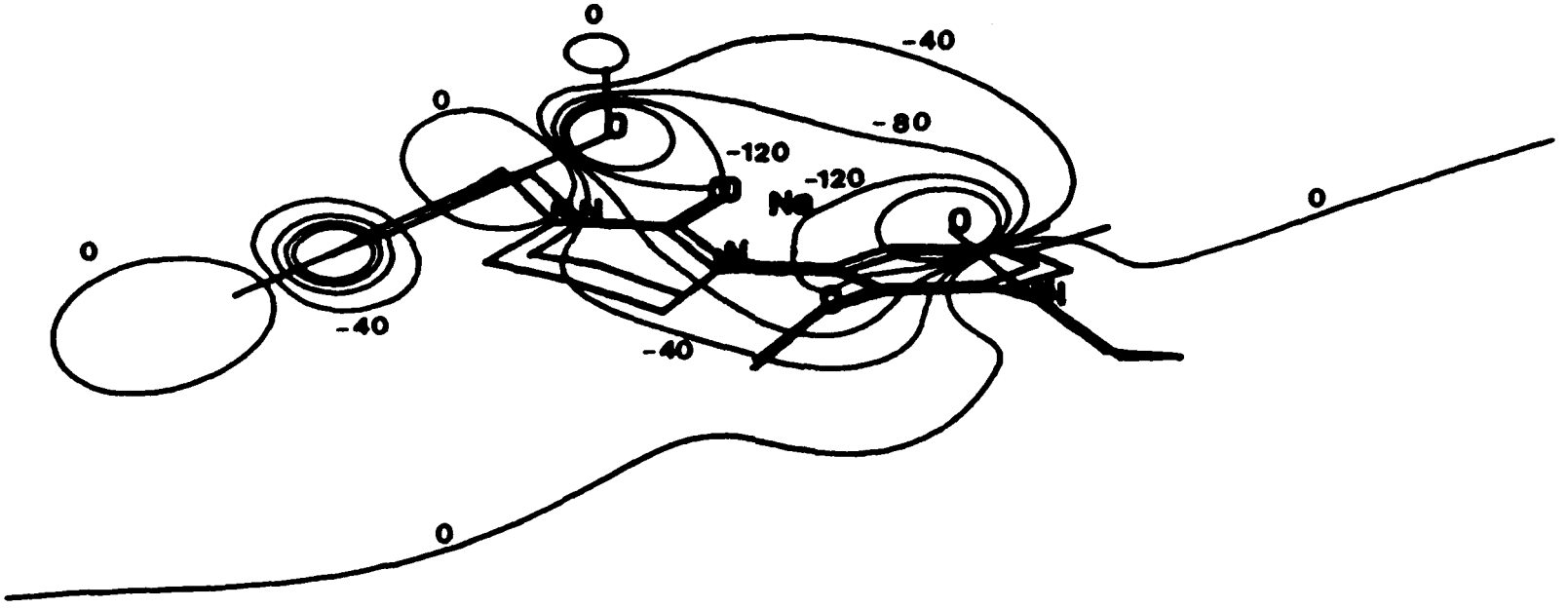

Fig. 11

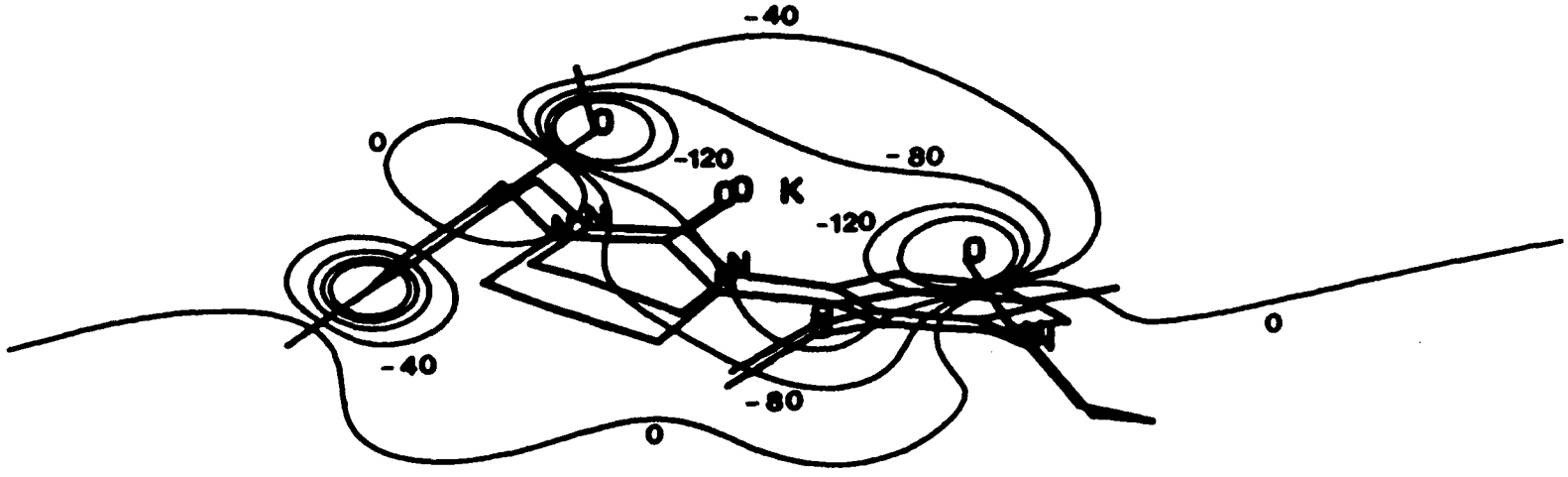

Fig. 12

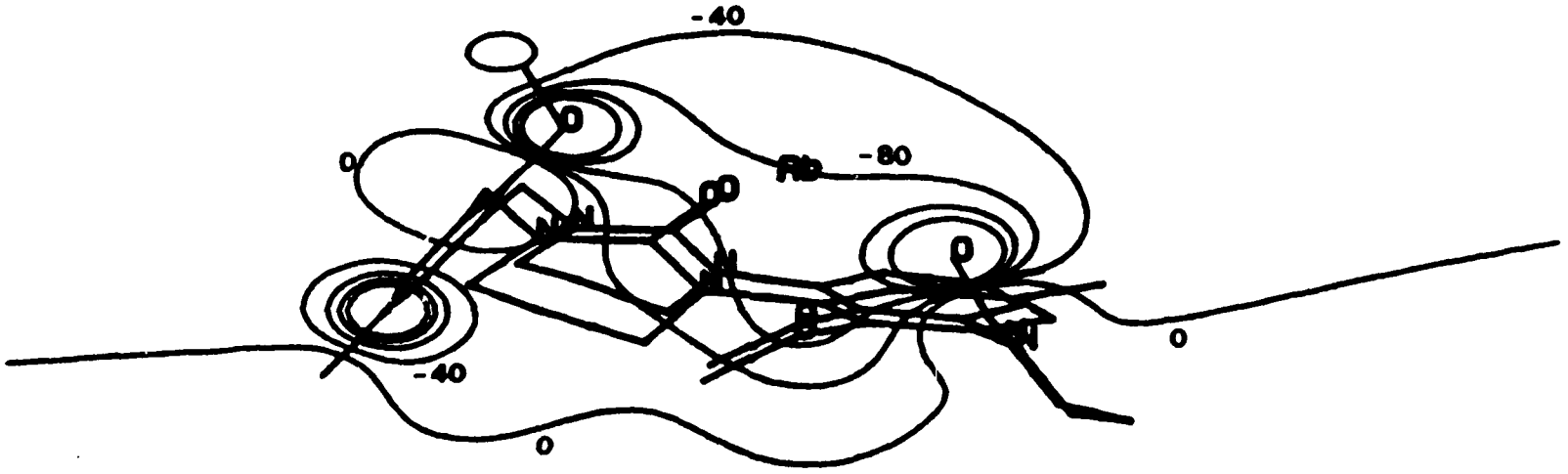

Fig. 13

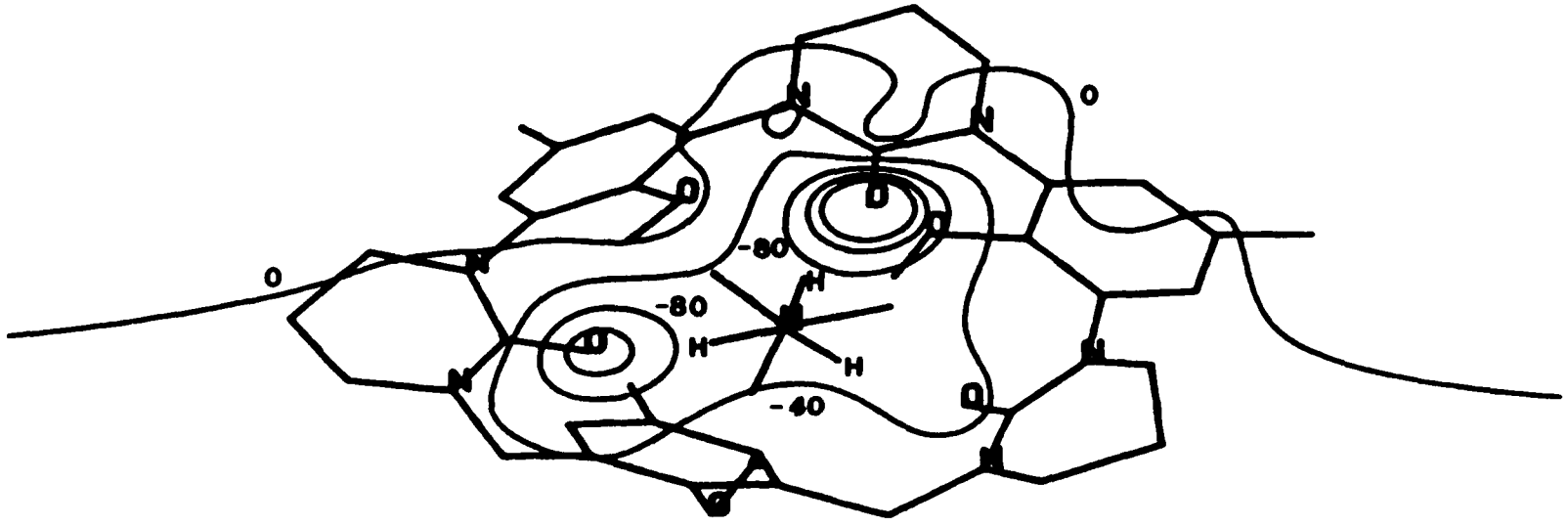

Fig. 15

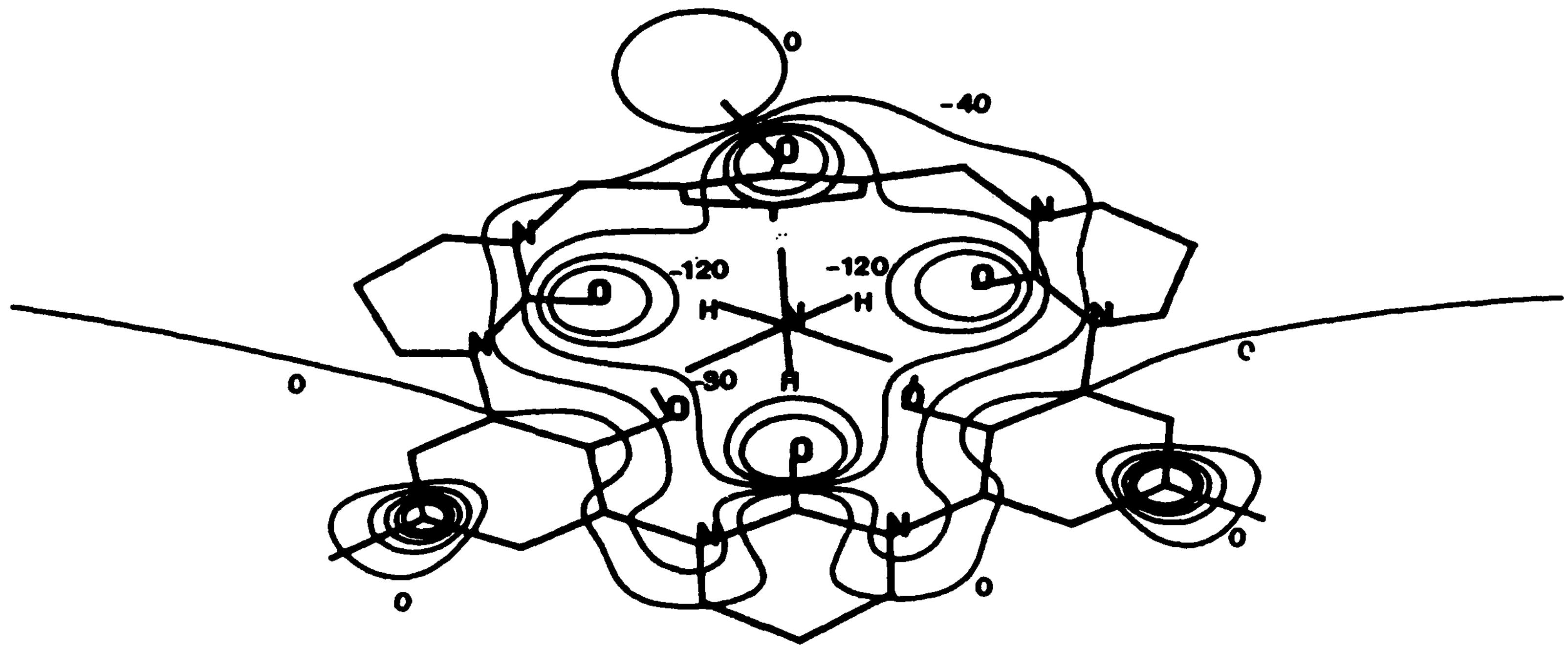

Fig. 16

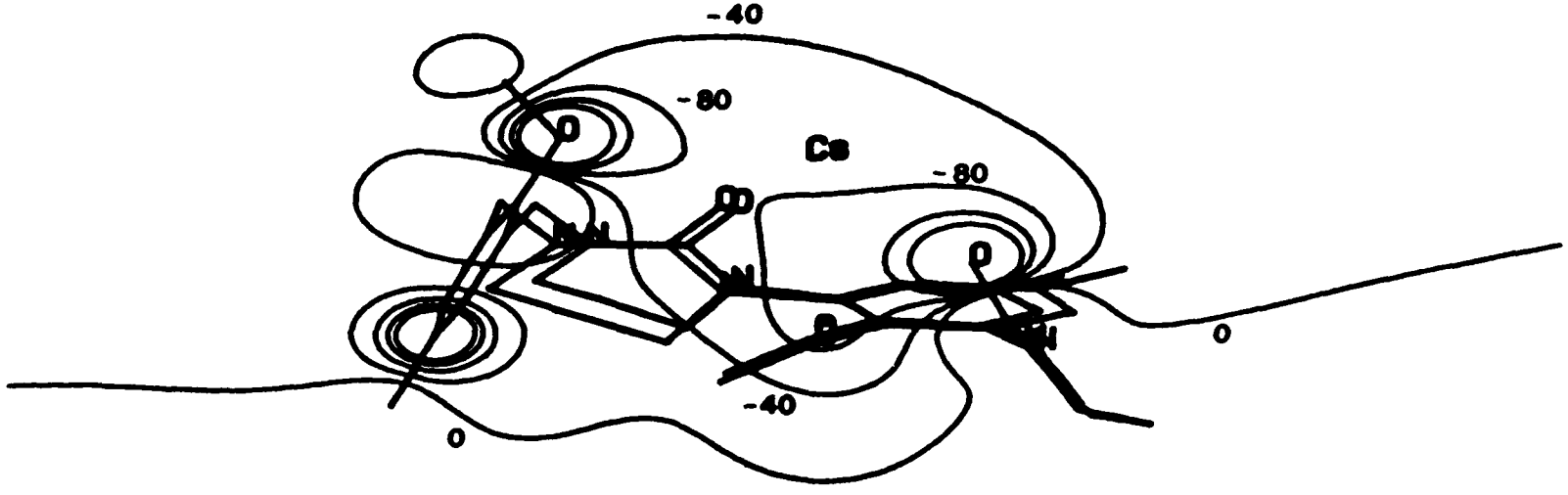

Fig. 14